Journal of CO_2 Utilization 22 (2017) 81–90

Contents lists available at ScienceDirect

Journal of CO_2 Utilization

journal homepage: www.elsevier.com/locate/jcou

Fly ash-derived MCM-41 as a low-cost silica support for polyethyleneimine in post-combustion CO_2 capture

R. Panek[a], M. Wdowin[b,*], W. Franus[a], D. Czarna[b], L.A. Stevens[c], H. Deng[c], J. Liu[c], C. Sun[c], H. Liu[c], C.E. Snape[c]

[a] Department of Geotechnics, Civil Engineering and Architecture Faculty, Lublin University of Technology, Nadbystrzycka 40, 20-618 Lublin, Poland
[b] Mineral and Energy Economy Research Institute, Polish Academy of Sciences, Wybickiego 7A, 31-261 Kraków, Poland
[c] University of Nottingham, Faculty of Engineering, Energy Technologies Building, Jubilee Campus, Nottingham NG7 2TU, United Kingdom

ARTICLE INFO

Keywords:
Fly ash
Rice husk ash
Mesoporous materials
CO_2 adsorption

ABSTRACT

The mesoporous silicate molecular sieve, MCM-41, has been synthesized from pulverized coal fly ash (PFA), where the silicate filtrate used is a by-product from hydrothermal zeolite production. Rice husk ash was also used for comparison but fusion with sodium hydroxide was used to prepare the silicate filtrate, along similar lines to earlier reports of using PFA as a precursor for MCM-41 synthesis. The MCM-41 samples are chemically and mineralogically similar to a commercially available sample, but with higher pore volumes dominated by mesopores (0.92–1.13 cf. 0.88 $cm^3 g^{-1}$). After polyethyleneimine (PEI) impregnation for CO_2 capture, the ash derived MCM-41 samples displayed higher uptakes than the commercial sample with the maximum achievable PEI loading of 60 Wt.% PEI (dry basis) before particle agglomeration occurs, approximately 13 compared to 11 Wt.%, respectively, the latter being comparable to earlier reports in the literature. The PFA sample that displays the fastest kinetics to achieve 90% of the equilibrium uptake had the largest mesopore volume of 1.13 $cm^3 g^{-1}$. Given the PFA-derived MCM-41 uses a waste silicate solution for hydrothermal preparation and no prior preparation is needed, production costs are estimated to be considerable lower where silicate solutions need to be prepared by base treatment, even if ash is used, as for the RHA derived MCM-41 used here.

1. Introduction

Anthropogenic carbon dioxide (CO_2) emissions from fossil fuel combustion are accepted as being major contributor to global warming, together with contributions from other greenhouse gases, methane, nitrous oxide (N_2O), water vapor, hydrofluorocarbons, perfluorocarbons, and sulfur hexafluoride [1]. Power generation accounts for 30% of global CO_2 emissions and there is an urgent need to deploy carbon capture and storage (CCS) to both conventional pulverized fuel coal-derived and natural gas combined cycle power plants globally, as well to major industrial emitters, including iron & steel and cement production.

Currently, CO_2 absorption with aqueous amine solutions (monoethyleneamine, MEA that can be used with secondary and tertiary amines) is the only mature capture technology having been used in natural gas separation for over 60 years, where recovery of CO_2 is at the level of 98% efficiency [2]. However, currently, the process is far from being completely cost effective due to the high energy requirement and the impact of solvent degradation and corrosion and high rates of water consumption. The cost of CO_2 capture for amine solutions in CCS technology can constitute 75% of the total cost of CO_2 sequestration [3–5]. Therefore, the development of next generation capture technologies with significantly lower energy penalties than amine scrubbing has been identified as a high priority area in the recent CCS roadmaps, for example in the UK (APGTF) [6], USA (DOE/NETL) [7], U.S. Department of Energy [8] and by the International Energy Agency (IEA) [9].

An alternative to amine scrubbing for post combustion capture (PCC) is using solid adsorbents, numerous materials have been tested including activated carbons (ACs) (prepared and modified by using reagents such as, KOH, K_2CO_3, $ZnCl_2$) [10,11], metal organic frameworks [12,13], microporous polymers [14], covalent organic frameworks [15] and supported amines [16]. Amines grafted or impregnated on aluminsilicates have been extensively researched due to their high CO_2 uptakes in dry and moist flue gases with CO_2 at low partial pressures. More specifically, polyethyleneimine (PEI) has been the most widely investigated impregnated amine based adsorbent [17–24] with it displaying fast adsorption kinetics at temperatures of *ca.* 75 °C.

* Corresponding author.
E-mail address: wdowin@meeri.pl (M. Wdowin).

http://dx.doi.org/10.1016/j.jcou.2017.09.015
Received 28 July 2017; Received in revised form 10 September 2017; Accepted 20 September 2017
Available online 06 November 2017

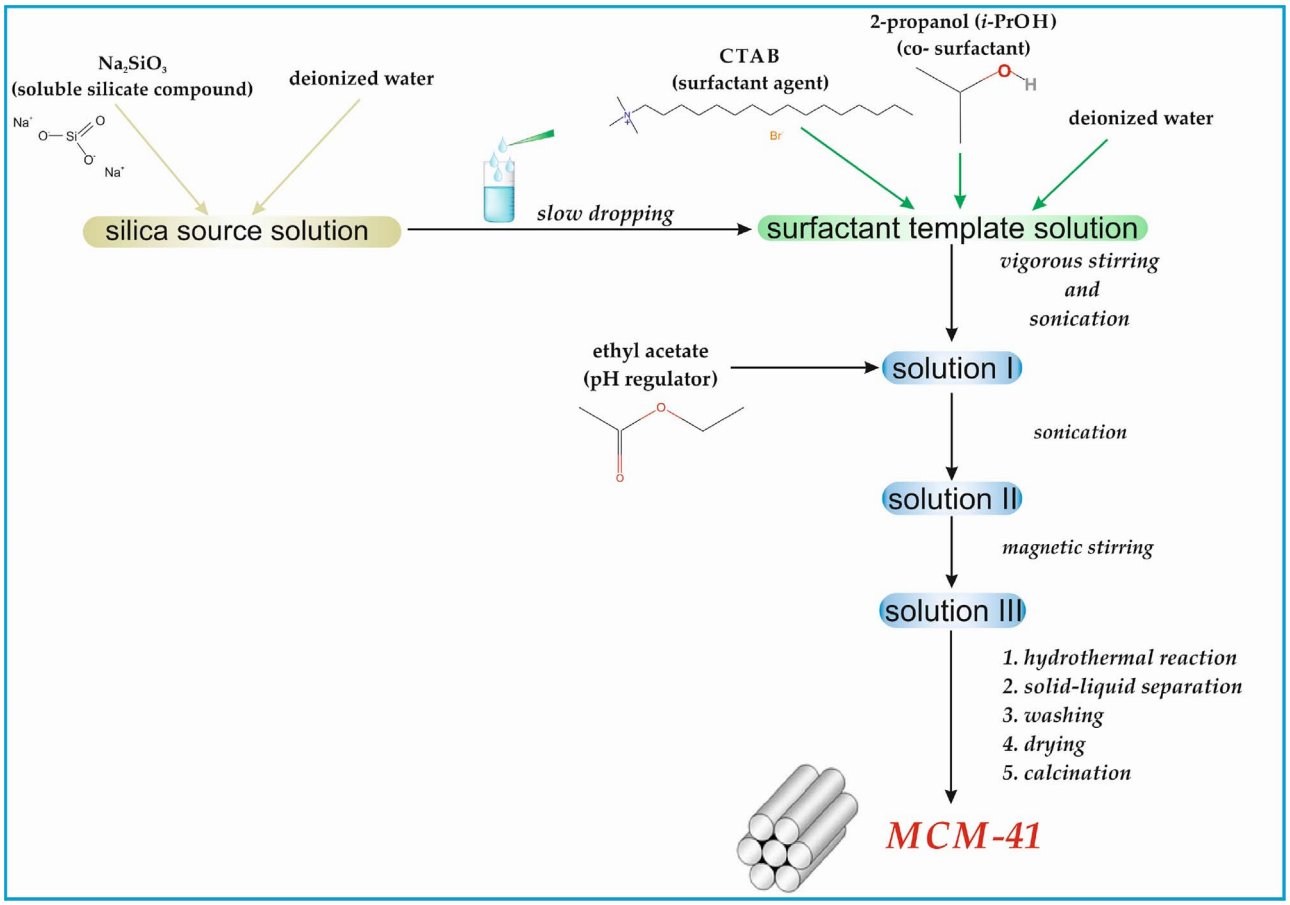

Fig. 1. Scheme of hydrothermal synthesis for MCM-41 [33].

Previous work has shown that the stability of PEI is extremely high during circulating fluidised bed operation over long operating periods provided that there is moisture both in the flue gas and in the sweep gas to remove CO_2 during regeneration at temperatures close to 130 °C [23]. However when considering scale-up, clearly the cost of mesoporous aluminosilcates used for PEI impregnation is a major consideration. Commercially available mesoporous silicas, MCM-41 and SBA-15 have all been found to be effective supports allowing PEI loadings of 50 wt.% or higher to be used [25,26]. Here we consider how the cost of MCM-41 can be reduced significantly by using a silicate solution which is a by-product from hydrothermal synthesis of zeolites using pulverized fly ash (PFA) from coal combustion.

MCM-41 is synthesized from silicate solutions using hydrothermal synthesis as depicted in Fig. 1 via a liquid templating mechanism [27–32]. The conventional synthesis using commercially available sodium silicate and a cationic surfactant, such as hexadecyltrimethylammonium bromide (CTAB) and a pH regulator is depicted in Fig. 1 [33]. After the hydrothermal reaction, the resultant MCM-41 is separated by filtration, dried and then surfactants are removed by calcination at temperatures in the range of 500–550 °C. Given that the current cost of MCM-41 from commercial suppliers is prohibitively expensive for the purity required for CO_2 capture, inexpensive sources of silicate are required to help reduce the overall production costs.

Inexpensive silica sources for base extraction that have received attention include fly ash from pulverised coal combustion (PFA) as well as rice husk ash (RHA) [34–38]. In the preparations of MCM-41 from PFA fly ash proposed by Majchrzak-Kucęba et al. [35] and Zhou et al. [38], the extraction of silicate is clearly necessary. Majchrzak-Kucęba et al. [35] used high temperature fusion of fly ash with NaOH, with the resulting sinter being mixed with water. In contrast, Zhou et al. [38] used the hydrothermal reaction of fly ash with NaOH solution, in an autoclave for 1 h at 100 °C. The second stage reported by Majchrzak-Kucęba et al. [35] used an appropriate amount of the surfactant CTAB at a pH of 11. Zhou et al. [38] used the same surfactant but with the addition of ethyl acetate as a pH regulator. There was also a small difference in the reaction temperature (Majchrzak-Kucęba et al. [35] used 100 °C and Zhou et al. [38] used 90 °C). Calcination in both cases was carried out 550 °C. The route proposed by Hui et al. [39] for PFA used NaOH solution at 100 °C for silicate extraction. The subsequent hydrothermal stage used CTAB as the surfactant, regulating pH with sulfuric acid but with the reaction being carried out at ambient temperature.

The aim of this study is to compare the structures of MCM-41 prepared from PFA and RHA and, then after PEI impregnation, compare their effectiveness for CO_2 capture with a commercial sample that has been prepared conventionally. The PFA preparation used waste silicate solution from the hydrothermal synthesis of zeolites for the first time and the potential cost reductions are considered. The CO_2 uptakes achieved are compared with those reported in other studies using conventional silicate sources for MCM-41 [25,26,35].

2. Materials and methods

To synthesise mesoporous MCM-41, RHA prepared by laboratory-scale combustion and a PFA from a Polish power plant were used (Kozienice Power Plant, Kozienice, Poland). The PEI used with a number average weight (M_w) of 800 was purchased from Sigma Aldrich (100 g) as was the commercial MCM-41 sample (25 g).

2.1. Chemical analysis

The chemical compositions of both starting material (PFA and RHA)

and the MCM-41 products were determined by X-ray energy dispersive fluorescence spectrometer (XRF, PANalytical Epsilon 3 spectrometer). The tests were carried out on the range of Na-Am (sodium to americium) and the instrument equipped with X-ray tube Rh 9W, 50 kV, 1 mA, 4096-channel spectrum analyzer, 6 measurement filters (Cu-500, Cu-300, Ti, Al-50, Al-200, Ag), the high-solid state detector SDD (Be window, a thickness of 50 µm) cooled by a Peltier cell.

The main elements in the filtrates were determined with Inductively Coupled Plasma Mass Spectrometry (ICP-MS, ELAN DRC-e Perkin Elmer instrument), the detection limits being below 0.01 mg/dm^3 for the metals analysed.

2.2. Synthesis of MCM-41

MCM-41 samples PFA-1 and PFA-2 were synthesized from the silicate-rich filtrate by-product obtained after hydrothermal synthesis of zeolites (20 kg of fly ash, 12 kg NaOH, 90 dm^3 of H_2O, temperature 80 °C, duration 36 h to prepare Na-P1 zeolite) using the apparatus described by Wdowin et al. [40] However, similar results should be obtained from waste silicate solution from synthesising other zeolites. For the RHA, the Si-rich filtrate was obtained by fusing 12.5 g of the RHA with 15 g NaOH (mass ratio of 1:2) at 550 °C for one hour, heating at 1 °C/min, as proposed by Majchrzak-Kucęba et al. [35]. The resulting sinter was mixed with water using at mass ratio of 4:1. The chemical composition of the filtrates from the PFA and RHA are presented in Table 1 which indicates that Si and Sodium (Na) dominate in both cases. There is some potassium (K) present for the PFA but not the RHA. With the exception of S and P arising from dissolved sulphate and phosphates, the concentrations of the minor and trace metals present, including Al, are all below 0.5% of the Si concentrations.

The subsequent MCM-41 hydrothermal synthesis for both PFA and RHA was carried out by the method modified by Majchrzak-Kucęba et al. [35] with CTAB as the surfactant. For PFA 1 and 2, 110 ml of filtrate was used with 5 g of CTAB, the reaction times differing being 96 and 72 h, respectively. This produced 2.5 and 2.6 g of MCM-41 respectively. From 34 ml of the RHA-derived silicate solution with 2.5 g of CTAB, 1.8 g of MCM-41 was obtained after a reaction time of 72 h.

Table 1
Compositions of the silicate-rich filtrates used for MCM-41 synthesis determined by ICP-MS.

Element	PFA (mg/dm^3)	RHA (mg/dm^3)
Al	92.6	135.9
As	9.7	3.1
B	1.6	< 0.1
Ba	0.5	< 0.1
Cd	0.3	< 0.1
Cr	0.1	4.6
Cs	0.5	< 0.1
Cu	0.7	1.0
Fe	21.7	44.1
Ga	2.8	< 0.1
Hg	0.3	< 0.1
K	2696.0	< 0.1
Li	4.9	< 0.1
Mg	0.9	171.8
Mn	0.3	< 0.1
Mo	5.5	< 0.1
Na	48759.0	63041.0
P	1425.0	1405.0
Pb	1.3	< 0.1
Rb	17.7	< 0.1
S	542.0	665.0
Se	less than 0.1	49.8
Sb	0.3	< 0.1
Si	36682	63263
Sn	63.3	52.1
Sr	0.3	< 0.1
Ti	7.1	< 0.1
U	0.4	< 0.1
V	32.8	< 0.1
W	4.0	< 0.1
Zn	2.5	< 0.1
Zr	2.3	< 0.1

Table 2
Ash compositions determined by XRF.

Compound	Concentration [Wt.%]	
	RHA	*PFA*
MgO	0.697	1.155
Al_2O_3	0.520	26.105
SiO_2	86.632	52.980
P_2O_5	2.287	2.290
SO_3	0.869	0.660
K_2O	5.907	3.445
CaO	1.879	2.904
TiO_2	0.035	1.841
Cr_2O_3	0.011	0.047
MnO	0.675	0.053
Fe_2O_3	0.331	7.675
NiO	0.005	0.040
CuO	0.005	0.033
ZnO	0.027	0.037
As_2O_3	0.001	0.008
Rb_2O	0.007	0.024
SrO	0.002	0.184
ZrO_2	0.001	0.086
Ag_2O	0.031	0.097

2.3. PEI impregnation and measurement of loadings

The desirable amount of PEI from a 50% aqueous solution was dissolved in 10 ml water with vigorous stirring for 15 min. Next, the corresponding amount of calcined mesoporous silica was gradually poured into the solution. The mixture was stirred overnight at room temperature and then dried at 40 °C in a vacuum oven for 24 h.

The theoretical PEI loading on a dry basis is defined as:

$$PEI\ loading\ (Wt.\ \%) = \frac{WPEI}{WPEI + W\ Silica} \times 100 \quad (1)$$

where W refers to the mass fractions on a dry basis.

The actual amount of PEI impregnated was determined by TGA (TA Instruments TGA Q500). Approximately 20 mg of sample was placed onto a platinum pan, the temperature was raised from ambient to 115 °C at a heating rate of 30 °C/min in pure nitrogen (N_2) gas (1 bar, 100 ml/min) and held isothermally for 30 min to remove moisture. Then, the temperature was cooled to approximately 90 °C, the gas switched to air (atmospheric pressure, 100 ml/min) and the temperature was ramped at 30 °C/min to 800 °C and held isothermally for 30 min. Weight% (Wt.% PEI loadings) were calculated on a dry basis determining the weight change between 150 and 700 °C, the temperature range over which PEI decomposed with devolatilisation and subsequent combustion of the volatiles. Samples were ran in duplicate with blank pan correction.

2.4. Mineralogical analysis of MCM 41 samples

Powder X-ray diffraction (XRD) (Panalytical X'pert APD diffractometer) was used with the data being processed by Philips X'Pert and ClayLab ver. 1.0 software. The identification of mineral phases was verified based on the PCPDFWIN ver. 1.30 database formalized by JCPDS-ICDD. The morphology and chemical composition of the main mineral components were investigated using an FEI Qanta 250 FEG scanning electron microscopy and energy dispersive spectroscopy (SEM/EDAX).

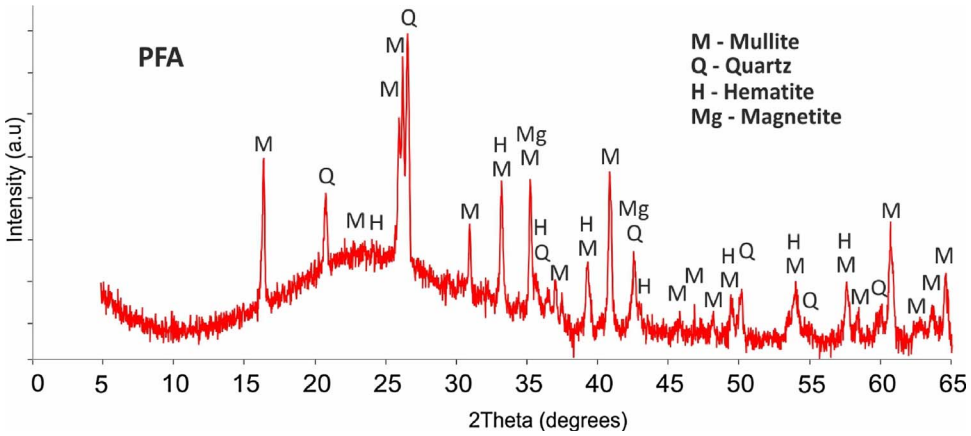

Fig. 2. XRD diffraction pattern of fly ash (PFA).

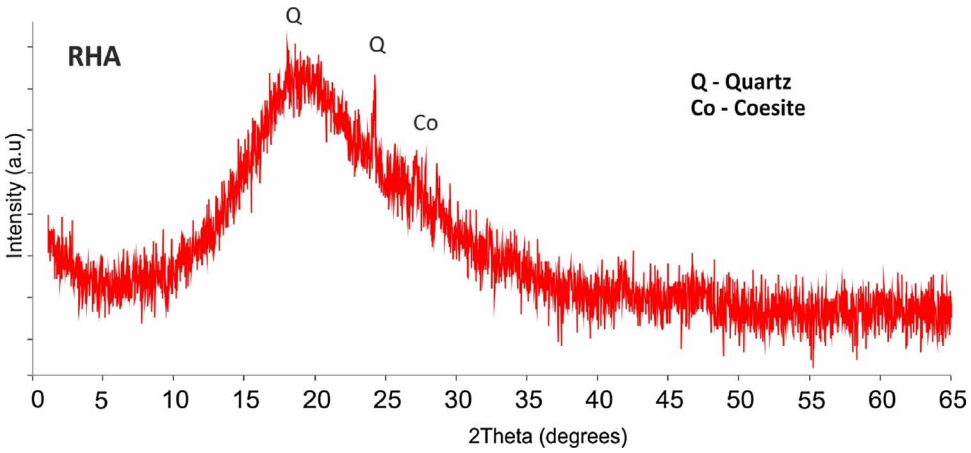

Fig. 3. XRD diffraction pattern of rice husk ash (RHA).

2.5. Textural characterisation

Textural properties were determined using a Micromeritics ASAP 2420 using N_2 as the adsorbate at −196 °C. N_2 sorption isotherms were acquired from 0.01 to 0.99 relative pressure (P/P_0). Approximately 0.2 g of sample was weighed into a sample tube and degassed at 250 °C for 24 h. The BET specific surface area was determined based on the SBET multilayer adsorption model, where P/P_0 was between 0.05 and 0.20 giving positive BET constants. The total pore volume (V_p) was determined from the adsorbed nitrogen volume at $P/P_0 = 0.99$. Average pore diameters (D_p) were calculated according to $Dp = 4\,V_p/SBET$. Mesopore volumes were calculated by using BJH adsorption model (Harkins Jura thickness equation) between 2 and 50 nm.

2.6. CO_2 adsorption

The CO_2 uptakes of the PEI impregnated adsorbents were determined by TGA Q500. Approximately 20 mg was weighed on to a platinum pan and was preheated to 115 °C at a heating rate of 30 °C/min in pure N_2 gas (1 bar, 100 ml/min), and held isothermally for 30 min to remove moisture. After the moisture removal stage, the temperature was lowered to the adsorption temperature of 75 °C and the gas switched to 15% CO_2 balanced by N_2 (1 bar, 100 ml/min) and held for 60 min to achieve adsorption equilibrium. CO_2 uptake (Wt.%) was determined through the weight difference between initial dry mass and mass after adsorption as shown in Eq. (2). Samples were analysed in duplicate, with blank pan correction.

$$Wt.\ \%CO_2\ uptake = \frac{Wfinal - Winitial}{Winitial} \times 100 \quad (2)$$

Rates of adsorption (kinetics) were assessed from the CO_2 adsorption isotherms, by recording the times taken to reach 30, 60, 90 and 95% of the full equilibrium capacities at 60 min.

3. Results and discussion

3.1. Ash characteristics

The RHA is characterised by a very high content of Si (*ca.* 87 Wt.%, Table 2), the remaining oxides being mainly Calcium (Ca), K and P with small amounts of aluminium (Al), magnesium (Mg), iron (Fe) and sulphur (SO_3). The PFA has a lower Si content than for RHA, approximately 53 Wt.%, with the Si to Al ratio being close to 2, with a significant amount Fe present (8 Wt.%). Oxides of K, Ca, Mg, Ti, together with SO_3, account for the remainder.

From XRD analysis both ash samples observed a very high background level of XRD diffraction curves (Figs. 2 and 3), indicating a high proportion of amorphous Si phases as well as quartz. For PFA (fly ash), a large degree of Fe components are observed, such as magnetite, hematite and mullite. For RHA the main mineral phase is abundantly Si related, such as silica glass, quartz and a polymorphic form coesite, this coincides with the data from XRF showing that RHA is predominately SiO_2.

Further, the ashes have very different morphological forms (Fig. 4). PFA comprises uniform spherical grains (pleospheres) with some agglomeration evident (Fig. 4a) on the surface, ranging from approximately 2–30 µm. For RHA (Fig. 4b), grains of non-uniform irregular shapes, larger than for PFA are evident, with a large amount of shapeless agglomeration of Si on the surface.

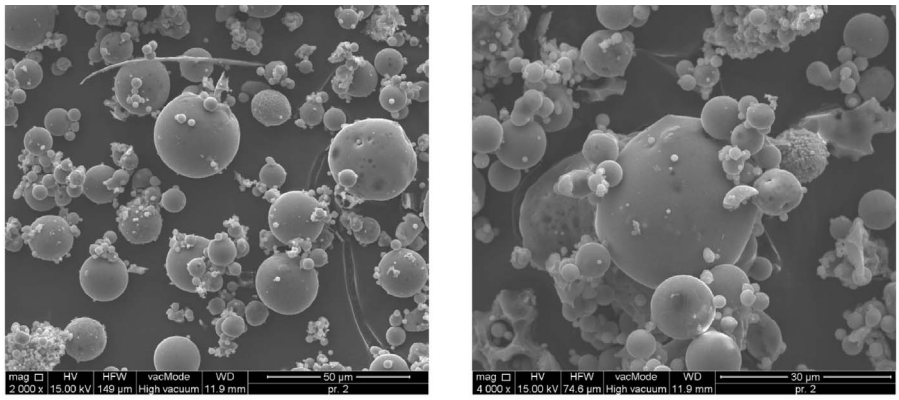

a) PFA (Fly ash)

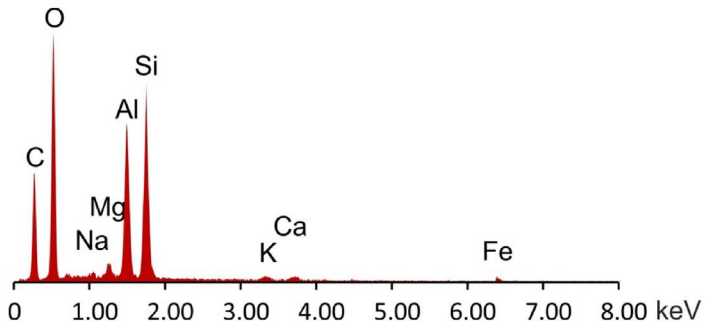

b) EDS analysis of PFA surface

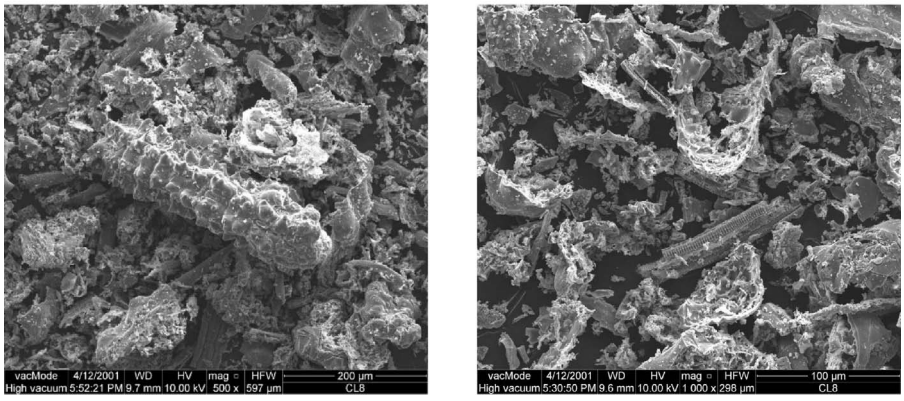

c) EDS analysis of RHA surface

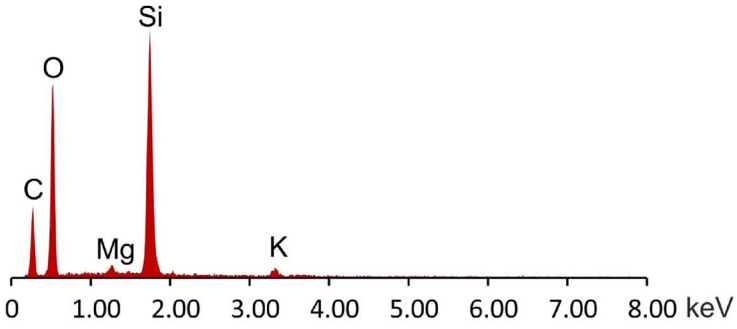

d) EDS analysis of agglomeration of Si on the RHA surface

Fig. 4. SEM microphotographs of (a) PFA – mag. 2000× (left) and 4000× (right), (b) EDS analysis of PFA surface (c) RHA mag. 500× (left) and 1000× (right) and (d) EDS analysis of RHA surface.

3.2. Characteristics of the MCM-41 samples

Table 3 indicates that the MCM-41 samples PFA-1 and PFA-2 approximately 97 Wt.% as SiO_2. Considerable amounts of Na_2O and Al_2O_3 are evident (ca. 1 to Wt.%). Other components were all less than 1 Wt.%. The RHA sample (RHA-1) has similar SiO_2 and Na_2O contents. The commercial MCM-41 has a lower measured content of silica (90 Wt.%), but this is likely to be experimental error since there is less Na_2O and no

Table 3
Compositions of the MCM-41 samples determined by XRF.

Compound	PFA-1 *Conc. [Wt.%]*	PFA-2 *Conc. [Wt.%]*	RHA-1 *Conc. [Wt.%]*	MCM-41 *Conc. [Wt.%]*
Na_2O	1.340	1.162	1.045	0.000
MgO	0.008	0.008	0.449	0.000
Al_2O_3	0.951	0.790	0.754	0.502
SiO_2	96.756	97.064	96.573	90.217
P_2O_5	0.439	0.417	0.443	0.000
SO_3	0.148	0.236	0.322	0.000
Cl	0.005	0.003	0.005	0.000
K_2O	0.010	0.018	0.007	0.005
CaO	0.120	0.103	0.249	0.000
TiO_2	0.026	0.021	0.004	0.016
V_2O_5	0.033	0.049	0.001	0.000
Cr_2O_3	0.001	0.001	0.001	0.000
MnO	0.002	0.002	0.010	0.000
Fe_2O_3	0.145	0.117	0.120	0.030
CuO	0.006	0.004	0.003	0.000
ZrO_2	0.000	0.000	0.000	0.007
Ag_2O_3	0.000	0.000	0.000	0.018
ZnO	0.009	0.006	0.014	0.000

Al_2O_3 compared to the PFA samples.

Fig. 5 shows that all the MCM-41 samples have very similar XRD profiles. The identification of the MCM-41 phase is based on the main d-spacing d_{hkl} = 40.71, 23.56, 20.31, 15.26 Å. Some very small shifts of peaks in the PFA and RHA-derived samples are evident, arising from the slightly higher levels of impurities.

Fig. 6 shows SEM microphotographs and accompanying EDS analysis for MCM-41 sample PFA-1. All three samples display very similar morphology approaching spherical and partially elongated shapes about size of 0.2 µm. Since all cases, EDS confirms the high silica contents. The high content of carbon arises from the coating to achieve better conductivity of electrons and reduce charging.

N_2 sorption isotherms of the MCM-41 samples are all type IVb, indicative of adsorbents with narrow mesopores. A steep rise in the amount of N_2 adsorbed can be observed between 0.3–0.4 P/P_0 that is common in MCM-41. On closer inspection, a slight hysteresis is observed in this region for the ash derived MCM-41 samples that is close to H1 hysteresis [41] which has been reported in templated mesoporous silicas such as MCM-41 and 48. However, all the MCM-41 samples have excellent pore uniformity due to little hysteresis, indicating little or no ink bottle pores.

Table 4 indicates that all MCM-41 samples are predominantly mesoporous, with mesopores accounting for over 90% of the total pore volume. PFA-1 has the highest BET specific surface area and pore volume, although the overall range of values for BET specific surface areas, total pore volume and mesopore volumes is relatively small. This might be explained by the longer reaction time of 96 h used in the hydrothermal synthesis for PFA-1 compared to 72 h for PFA-2 and RHA-1. Overall, RHA-1 is very similar to the commercial MCM-41 sample, with the proportion of mesopores accounting for slightly less of the total pore volume (91–92%) than for the two PFA samples (95–98%, Table 4).

3.3. PEI loadings

The TGA profiles of the impregnated MCM-41 samples displayed sharp weight decreases up to 115 °C due to moisture (Fig. 7 for the commercial and PFA-1 derived samples). Although the samples were pre-dried for 24 h in a vacuum oven at 40 °C, this was not a high enough temperature to remove all the moisture due to association with the PEI and surface silanol groups, coupled with the fact the samples re-equilibrate with moisture on exposure to the atmosphere. Another noticeable drop in mass occurs around 150 °C attributed to the volatilisation of low molecular mass PEI oligers. Thermal decomposition and combustion of the remaining PEI occurs and this continues up to 700 °C where only the silica substrate remains.

The PEI loadings determined form TGA are listed in Table 5. All the measured PEI loadings are comparable to the theoretical values. All of the MCM-41 impregnated samples are free flowing powders up to 60 Wt.%, but above this point, samples become heavily agglomerated and adhesive, as PEI starts to cover the surface of particles.

3.4. CO_2 adsorption and kinetics

CO_2 uptakes were determined by TGA in 15% CO_2 balanced by N_2 at 75 °C simulating PCC conditions from coal-fired power plant, within the temperature range found to be optimum for PEI by other researchers [18–23,35,42]. Fig. 8 presents the uptake profiles for the commercial and PFA-1-derived samples. CO_2 uptakes and with the times taken to reach 30 with 60 and 90% of the final uptakes after an hour are listed in Table 6.

The CO_2 uptake profiles are dominated by the rapid initial uptake that occurs in less than 4 min, followed by a much slower uptake that typically accounts for less than 20% of the final uptake reached after an hour. At the higher PEI loadings (50 and 60 Wt.%) for the commercial MCM-41, it is noticeable that the slower component tails more and does not appear to quite reach the limiting or equilibrium capacity within one hour (Fig. 8).

As is well established [24,25,35], CO_2 uptakes increase with PEI loading, as can be seen for the commercial MCM-41 going from 6.4 to 11.2 Wt.% as the PEI loading increases from 40 to 60 Wt.% (Fig. 8 and

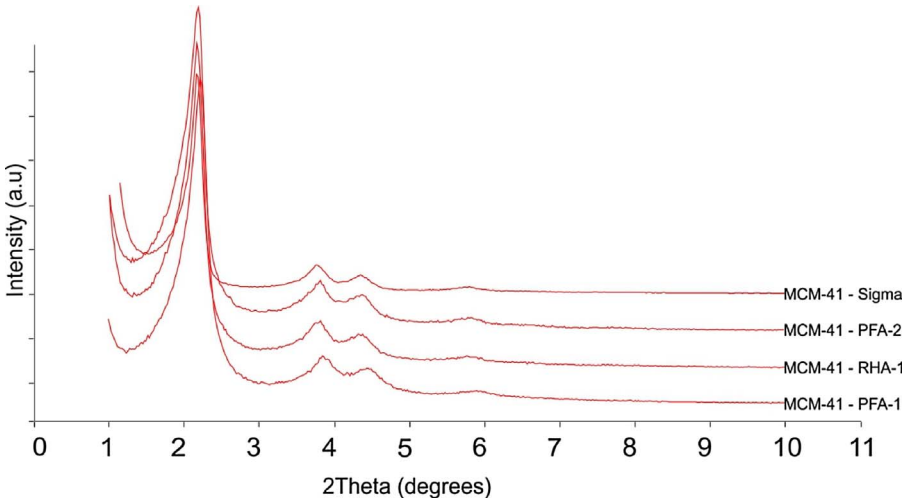

Fig. 5. XRD diffraction patterns of the MCM-41 samples.

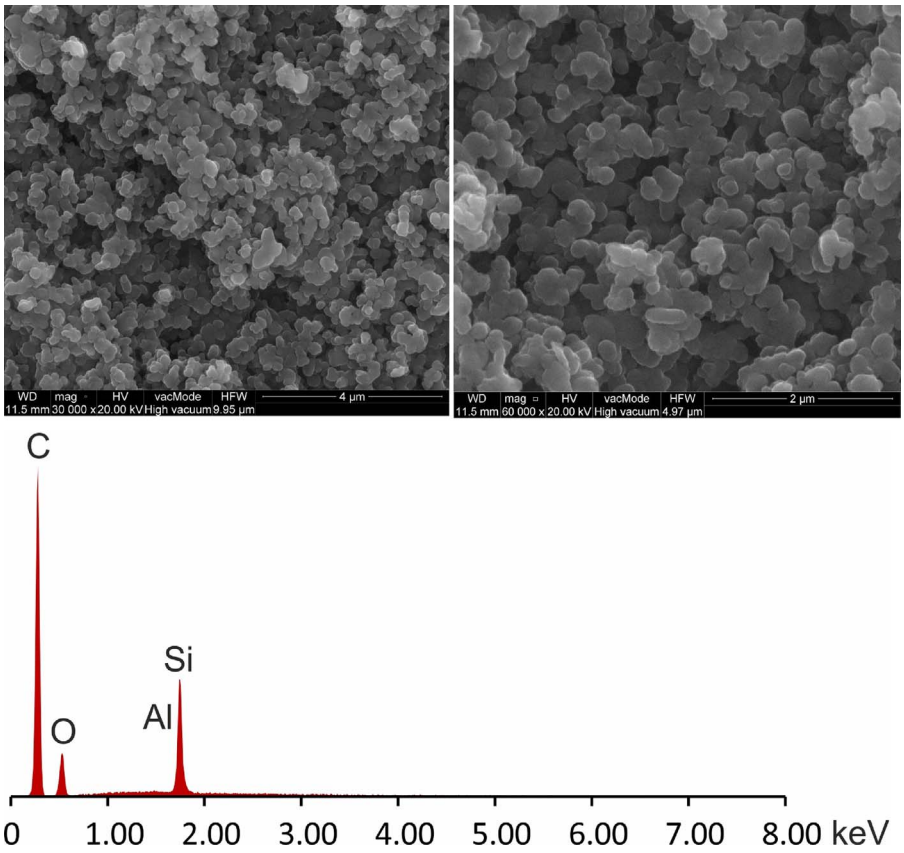

Fig. 6. SEM photomicrographs with EDS analysis of for MCM-41 PFA-1, mag. 30,000× (left) and 60,000× (right).

Table 4
Textural parameters of the MCM-41 samples.

SAMPLE	S_{BET} (m^2/g)	$V_{p\text{-total}}$ (cm^3/g)	V_{meso} (cm^3/g)	average pore diameter(nm)
MCM-41 Commerial	991	0.97	0.88 (91)[a]	3.92
MCM-41 (PFA-1)	1230	1.19	1.13 (95)[a]	3.88
MCM-41 (PFA-2)	1049	0.98	0.96 (98)[a]	3.74
MCM-41 (RHA-1)	980	1.00	0.92 (92)[a]	4.08

[a] Parenthesis denotes percentage porosity of mesopores ((Vmeso/Vp − total)*100).

Table 6). However, the results clearly indicate that the ash derived MCM-41 samples have considerably higher maximum CO_2 adsorption capacities at both 50 and 60 Wt.% PEI loading, probably attributable to the larger mesopore volumes (Table 4), 1.13, 0.96 and 0.92 $cm^3\,g^{-1}$ for PFA-1 and 2, RHA-1, respectively compared to 0.88 $cm^3\,g^{-1}$ for the commercial sample. As already indicated, increasing the loading further to 65 and 70 Wt.% gave samples that were adhesive and largely agglomerated with CO_2 uptakes falling to well below 10 Wt.%.

As well as giving higher CO_2 uptake, all three ash derived MCM-41 samples have superior kinetics compared to their commercial equivalent at 50 and 60 Wt.% PEI loading, with the times taken to reach 30, 60 and 90% CO_2 capacity (t_{30}, t_{60} and t_{90}, Table 6) occurs a lot faster than the commercial MCM-41. For example, for t_{90}, as it takes approximately 18 min for the commercial sample to reach 90% capacity, while the ash derived samples achieve this in less than 10 min. All three ash derived MCM-41 samples display comparable adsorption kinetics at t_{30} and t_{60}, but MCM-41 PFA-1 60% has faster kinetics for t_{90}, 7.6 compared to 9.53 and 9.2 min for PFA-2 and RHA-1. This could suggest that with the higher mesoporosity for PFA-1 (1.13 $cm^3\,g^{-1}$, Table 4), larger mesopores are more available and possibly interconnected to macropores and surface voids to aid gas diffusion.

3.5. Comparisons of CO_2 uptakes with other studies

Other researchers have reported on MCM-41 wet impregnated with PEI [21,25,35]. Xu et al. synthesised MCM-41 from sodium and ammonium silicates and report that 50 Wt.% PEI loading (dry basis) gave the highest CO_2 uptake of 11.2 Wt.% at 75 °C in one atmosphere of CO_2 which falls to approximately 9 and 10 Wt.% as the partial pressure is reduced to 0.1 and 0.3 atmospheres, respectively. These values appear to be comparable to those of 8.4 and 9.9 Wt.% obtained with 50 and 55% PEI loadings reported here (Table 6) with a partial pressure of 0.15 atmospheres for the commercial MCM-41 sample. The values reported by Xu et al. are comparable to that for PFA-2 with a 50% loading (8.8) but lower than that of obtained with the same loading for PFA-1 and RHA-1 (10.6 and 10.1 Wt.%, respectively).

Using the sample analysis conditions as Xu et al. [25], Majchrzak-Kucęba et al. [35] for fly ash-derived MCM-41 reported an uptake close to 10% at 75 °C with a 50% loading. This is again similar to the values reported here and the pore volume of this sample was 1.0 cm^3/g comparable to those for PFA-1 and RHA-1 with very similar pore volumes. Le et al. [26] also using a commercial MCM-41 observed that as PEI loading increases CO_2 capacity increases with an optimum loading of 50 Wt.% with a surprising low CO_2 uptake of around 2.5 Wt.% at an adsorption temperature of 40 °C. However, if mole% has been incorrectly reported as Wt.%, then the uptake reported would be ca. 10.5% which is close to the values just described.

Clearly, all the values reported here for the maximum achievable PEI loading of 60 Wt.% before particle agglomeration occurs, close to 13 Wt.% are all higher than those with a 50 Wt.% loading reported here and in the earlier studies [21,25,35]. As already discussed for a given PEI loading these relatively small differences can be attributed to differences in the mesopore volume arising from the synthesis routes used, but further work is required to fully explore how these differences might arise.

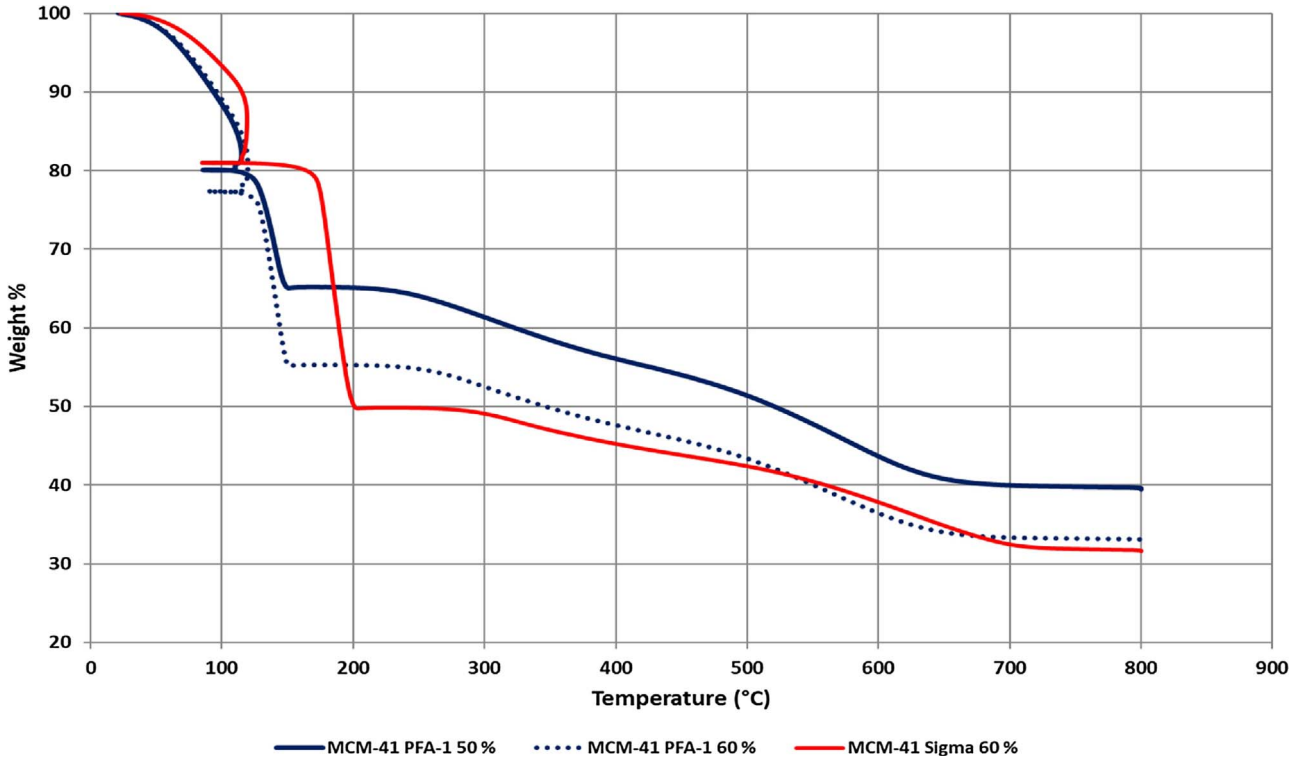

Fig. 7. TGA profile showing PEI loss for MCM-41 PFA-1 for the 50 and 60 Wt.% loading used, and MCM-41 Sigma 60 Wt.% as a comparison.

Table 5
Wt.% PEI loadings for the MCM-41 samples, actual PEI loading on a dry basis by TGA.

SAMPLE	Theoretical Loading (Wt.%)	Actual PEI loading (Wt.%)
MCM-41 Com 40%	40	38.04 ± 0.56
MCM-41 Com 50%	50	50.01 ± 0.93
MCM-41 Com 55%	55	55.42 ± 0.07
MCM-41 Com 60%	60	60.81 ± 0.24
MCM-41 PFA-1 50%	50	51.39 ± 0.96
MCM-41 PFA-1 60%	60	57.46 ± 0.24
MCM-41 PFA-2 50%	50	47.75 ± 0.33
MCM-41 PFA-2 60%	60	60.87 ± 0.36
MCM-41 RHA-1 50%	50	48.02 ± 1.86
MCM-41 RHA-1 60%	60	61.71 ± 0.22

Com = commercial.

3.6. Economic assessment

The PFA derived MCM-41 samples prepared from waste silicate solution offer considerable potential for reducing the overall cost of synthesis of this material. Indeed, the commercial fabrication of sodium silicate from quartz sand and sodium carbonate at 1300 °C requires a large input of energy [43,44]. The synthesis costs are even higher if organic silicon reagents are used for preparing mesoporous silicates [45,46]. In order to reduce the cost, a number of low-cost silica sources have been identified including natural zeolites [47], clay [48,49], ore tailoring [50,51], agriculture slag waste [52], E-waste [53], wheat husk [54], rice husk [37,55], as well as coal fly ash [38,56]. However, either fusion or autoclave treatment step with NaOH is still required with energy costs still being considerable.

Regarding the direct use of waste silicate solutions as used here for PFA, Shah et al. [57] used siliceous sugar industry waste but they employed a multistep extraction procedure to obtain a solution with the silicate content being similar to that used here.

The estimated cost for production at a laboratory scale of the PFA-derived MCM-41 is approximately 1200 euro per kg. This includes some equipment cost, but the largest operating costs are for reactants (approx. 1000 euro per kg), mainly for the surfactant, as well as energy, at approx. 2.5 euro/kWh, and labour costs. There is some savings on reagent costs because the synthesis does not require ethyl acetate as co-solvent as in case of Meléndez-Ortiz et al. [33]. As reported by Lawrence et al. [58], costs can be reduced by shortening time for MCM-41 synthesis but it was found here and in earlier work, that relatively long times are needed to obtain high purity MCM-41.

Compared to the cost of the waste-silicate solution-derived here, the cost of the commercial sample used here purchased on a small-scale runs to several tens of thousands of euros per kg, although clearly not produced on a kg scale. The only such sample we could identify (ACS Material LLC) is currently available at a cost of approximately 2000 euro per 1 kg [59] but this has lower purity than the commercial sample used here.

Regarding the potential application to PCC, it should be remembered that after prolonged usage in circulating fluidized-bed systems, provided that MCM-41-PEI has good attritional resistance as found for other mesoporous silicas [23], then it should be possible to recycle the silica where degraded PEI can be removed by controlled combustion. Therefore, provided the cost of recycling is low, the silica preparation costs can be considered largely as an initial cost whilst the cost of replenishing PEI will be a significant operating cost.

4. Conclusions

Fly and rice husk ash as low-cost silica sources have successfully been used for the synthesis of high purity MCM-41. Chemical and mineralogical analysis shows that the ash derived MCM-41 samples have similar chemistry to that of a commercial sample, with SEM showing identical morphologies between samples. However, the ash-derived samples have higher mesopore volumes than the commercial sample used (0.92–1.13 cf. 0.88 $cm^3 g^{-1}$).

After PEI impregnation for CO_2 capture, the ash derived MCM-41 samples displayed higher uptakes and faster kinetics at the maximum loading of 60 Wt.% PEI than the commercial sample, approximately 13 wt.% for PFA-1, PFA-2 and RHA-1 compared to 11 Wt.%,

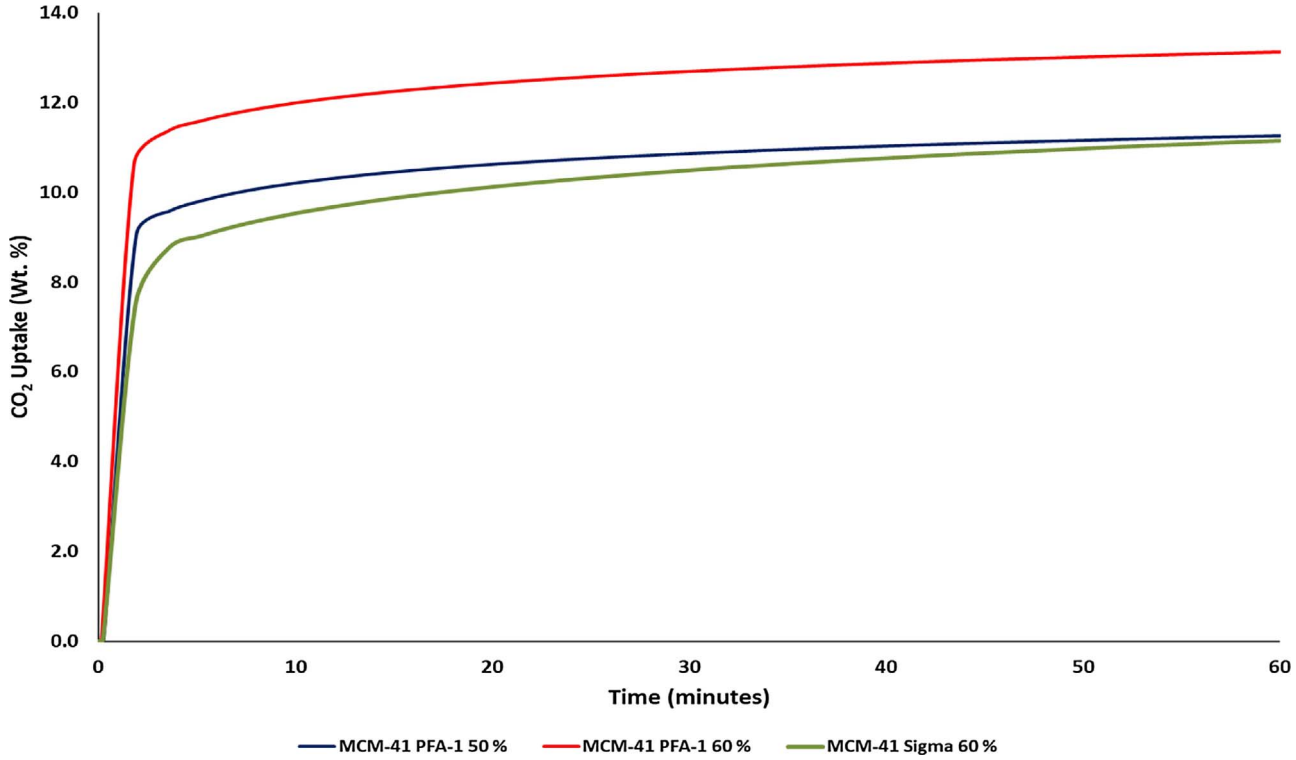

Fig. 8. CO_2 adsorption profiles for MCM-41 PFA-1 with 50 and 60 Wt.% PEI and MCM-41 Sigma 60% as a comparison.

Table 6
CO_2 uptakes and times to achieve 30, 60 and 90% uptakes in 15% CO2 at 75 °C for MCM-41 series of samples.

SAMPLE	CO_2 uptake (Wt.%)	Times for (minutes)		
		t_{30}	t_{60}	t_{90}
MCM-41 Com. 40%	6.44 ± 0.16	0.63 ± 0.16	0.95 ± 0.19	10.76 ± 0.58
MCM-41 Com. 50%	8.37 ± 0.22	0.58 ± 0.02	0.93 ± 0.07	19.36 ± 0.72
MCM-41 Com. 55%	9.92 ± 0.17	0.64 ± 0.01	0.97 ± 0.03	17.70 ± 0.04
MCM-41 Com. 60%	11.17 ± 0.04	1.01 ± 0.24	1.50 ± 0.32	17.50 ± 0.83
MCM-41 PFA-1 50%	10.64 ± 0.88	0.76 ± 0.24	1.08 ± 0.27	7.99 ± 1.27
MCM-41 PFA-1 60%	13.08 ± 0.06	0.74 ± 0.03	1.15 ± 0.04	7.64 ± 0.14
MCM-41 PFA-2 50%	8.79 ± 0.05	0.54 ± 0.01	0.80 ± 0.01	7.63 +0.09
MCM-41 PFA-2 60%	12.91 ± 0.09	0.71 ± 0.01	1.11 ± 0.04	9.53 ± 0.37
MCM-41 RHA-1 50%	10.13 ± 0.06	0.59 ± 0.02	0.88 ± 0.02	8.28 ± 0.16
MCM-41 RHA-1 60%	13.31 ± 0.09	0.68 ± 0.02	1.02 ± 0.06	9.20 ± 0.30

Standard deviations derived from duplicate measurements on each sample. Com = commercial.

respectively. At the maximum 60 Wt.% PEI loading, PFA-1 sample has the fastest adsorption kinetics to achieve 90% of the equilibrium uptake, attributed to it having the largest mesopore volume of 1.13 $cm^3\,g^{-1}$.

The use of PFA-derived waste silicate solution from synthesizing other zeolites has the potential to reduce production costs considerably for MCM-41 which are estimated to approximately 1200 euro per kg for the scale of the facility used here.

Conflict of interest

There are no conflict of interest to declare.

Acknowledgements

This work was supported by the Engineering and Physical Sciences Research Council [Grant number EP/L020777/1]; and the Polish National Centre Research and Development, within the framework of the FENCO-NET Grant no 231333, CO2 post-combustion capture using amine impregnated synthetic zeolites, contract NCBR/FENCO-NET 1/2013.

References

[1] S. Solomon, D. Quin, M. Manning, Z. Chen, M. Marquis, K.B. Avert, M. Tignor, H.L. Miller, Contribution of Working Group I to the Fourth Assessment Report Intergovernmental Panel on Climate, United Kingdom and USA, 2007.
[2] A. Yamasaki, J. Chem. Eng. Jpn. 36 (4) (2003) 361–375.
[3] D.J. Fauth, E.A. Frommell, J.S. Hoffman, R.P. Reasbeck, H.W. Pennline, Fuel Process. Technol. 86 (14–15) (2015) 1503–1521.
[4] J.T. Yeh, K.P. Resnik, K. Rygle, H.W. Pennline, Fuel Process. Technol. 86 (14–15) (2005) 1533–1546.
[5] H. Yang, Z. Xu, M. Fan, R. Gupta, R.B. Slimane, I. Bland, J. Environ. Sci. 20 (2008) 14–27.
[6] APGTF, Cleaner Fossil Power Generation in the 21st Century: Maintaining a Leading Role, UK, (2011).
[7] DOE/NETL, Carbon Dioxide Capture and Storage RD&D Roadmap, December, 2010.
[8] U.S. Department of Energy, Carbon Capture, Utilization, and Storage: Climate Change, Economic Competitiveness, and Energy Security, (2017) Accessed August, 2016 https://energy.gov/sites/prod/files/2016/09/f33/DOE%20-%20Carbon%20Capture%20Utilization%20and%20Storage_2016-09-07.pdf.

[9] IEA Carbon Capture and Storage Technology Roadmap, OECD/IEA, Paris, 2013.
[10] N.A. Rashidi, S. Yusup, L.H. Loong, Chem. Eng. Trans. 35 (2013) 361–366.
[11] J. Sreńscek-Nazzal, U. Narkiewicz, A.W. Morawski, R. Wróbel, A. Gęsikiewicz-Puchalska, B. Michalkiewicz, Acta Phys. Pol. A 129 (3) (2015) 394–401.
[12] D. Britt, H. Furukawa, B. Wang, T.G. Glover, O.M. Yaghi, PNAS 106 (49) (2009) 20637–20640.
[13] R. Willis, A. Benin, J. Low, G. Venimadhavan, S. Faheem, D. Lesch, D. Matzger, R. Snurr, Technical Report, 2008, Contract Number: DE-FG26-04NT42121.
[14] C. Xu, N. Hedin, Mater. Today 17 (8) (2014) 397–403.
[15] Y. Zheng, R. Zou, Y. Zhao, Adv. Mater. 28 (15) (2016) 2855–2873.
[16] T. Sakpal, A. Kumar, S.P. Kamble, R. Kumar, Indian J. Chem. Sect. 51 (9) (2012) 1214–1222.
[17] W.J. Son, J.S. Choi, W.S. Ahn, Microporous Mesoporous Mater. 113 (2008) 31–40.
[18] G. Qi, Y. Wang, L. Estevez, X. Duan, N. Anako, Ah-H. A. Park, W. Li, Ch.W. Jones, E.P. Giannelis, Energy Environ. Sci. 4 (2011) 444–452.
[19] A. Samanta, A. Zhao, G.K.H. Shimizu, R. Gupta, Ind. Eng. Chem. Res. 51 (2012) 1438–1463.
[20] J. Wang, L. Huang, R. Yang, Z. Zhang, J. Wu, J. Gao, Q. Wang, D. O'Hare, Z. Zhong, Energy Environ. Sci. 7 (2014) 3478–3518.
[21] K. Li, J. Jiang, F. Yan, S. Tian, X. Chen, Appl. Energy 136 (2014) 750–755.
[22] K. Li, J. Jiang, S. Tian, F. Yan, X. Chen, R. Soc. Chem. 3 (2015) 2166–2175.
[23] W. Zhang, H. Liu, C.G. Sun, T.C. Drage, C.E. Snape, Chem. Eng. J. 251 (2014) 293–303.
[24] N. Sun, Z. Tang, W. Wei, C.E. Snape, Y. Sun, Solid adsorbents for CO_2 capture with low energy penalties leading to integrated low carbon energy solutions, Front. Energy Res. 3 (2015) Article 9.
[25] X. Xu, C. Song, J.M. Andresen, B.G. Miller, A.W. Scaroni, Energy Fuels 16 (2002) 1463–1469.
[26] M.U.T. Le, S.Y. Lee, S.J. Park, Int. J. Hydrogen Energy 39 (2014) 12340–12346.
[27] C.T. Kresge, M.E. Leonowicz, W.J. Roth, J.C. Vartuli, J.S. Beck, Nature 359 (1992) 710–712.
[28] A. Monnier, F. Schuth, Q. Huo, D. Kumar, D. Margolese, R.S. Maxwell, G.D. Stucky, M. Krishnamurty, P. Petroff, A. Firoouzi, M. Janicke, B.F. Chmelka, Science 261 (1993) 1299–1303.
[29] M.A. Karakassides, A. Bourlinos, D. Petridis, L. Coche-Guerente, P. Labbe, J. Mater. Chem. 10 (2000) 403–408.
[30] S.P. Naik, A.S.T. Chiang, R.W. Thompson, J. Phys. Chem. B 107 (2003) 7006–7014.
[31] B.G. Trewyn, I.I. Slowing, S. Giri, H.T. Chen, V.S.Y. Lin, Acc. Chem. Res. 40 (2007) 846–853.
[32] K.M. Parida, S.S. Dash, J. Mol. Catal. A 306 (2009) 54–61.
[33] H.I. Meléndez-Ortiz, A. Mercado-Silva, L.A. García-Cerda, G. Castruita, Y.A. Perera-Mercado, J. Mex. Chem. Soc. 57 (2) (2013) 73–79.
[34] K.S. Hui, K.N. Hui, S.K. Lee, Int. J. Chem. Biol. Eng. 2 (4) (2009) 165–175.
[35] I. Majchrzak-Kucęba, D. Bukalak, W. Nowak, J. Ozonek, M. Pawłowska (Eds.), Polska inżynieria środowiska pięć lat po wstąpieniu do unii europejskiej. v. 1, Komitet inżynierii środowiska PAN, Monografie Nr 58, Lublin, 2009.
[36] T.Z. Liou, Chem. Eng. J. 171 (2011) 1458–1468.
[37] N.K. Renuka, A.K. Praveen, K. Anas, Mater. Lett. 109 (2013) 70–73.
[38] Ch. Zhou, Q. Gao, W. Luo, Q. Zhoua, H. Wang, Ch. Yan, P. Duan, J. Taiwan Inst. Chem. Eng. 52 (2015) 147–151.
[39] K.S. Hui, K.N. Hui, S.K. Lee, World Acad. Sci. Eng. Technol. J. Mech. Aerosp. Ind. (2009) 489–499.
[40] M. Wdowin, M. Franus, R. Panek, L. Bandura, W. Franus, Clean Technol. Environ. Policy 16 (6) (2014) 1217–1223.
[41] M. Thommes, K. Kaneko, A.V. Neimark, J.P. Olivier, F. Rodriguez-Reinoso, J. Rouquerol, S.W. Sing, Pure Appl. Chem. (2015), http://dx.doi.org/10.1515/pac-2014-1117.
[42] W.J. Son, J.S. Choi, W.S. Ahn, Microporous Mesoporous Mater. 113 (2008) 31–40.
[43] C.J. Brinker, G.W. Scherer, Applications, Sol-Gel Science: The Physics and Chemistry of Sol-Gel Processing, Academic Press, Inc, San Diego, CA, 1990.
[44] V. Narayanana, S. Daniel, S. Kannan, Mater. Res. 12 (4) (2009) 411–414.
[45] W.L. Dai, H. Chen, Y. Cao, H.X. Li, S.H. Xie, K.N. Fan, Chem. Commun. (2003) 892–893.
[46] Y. Zhang, L. Kang, J. Shang, H. Gao, J. Mater. Sci. 48 (2013) 5571–5578.
[47] S. Jin, K. Cui, H. Guan, M. Yang, L. Liu, C.L. Jin, C. Lan, Appl. Clay Sci. 56 (2012) 1–6.
[48] H. Yang, Y. Deng, C. Du, S. Jin, Appl. Clay Sci. 47 (2010) 351–355.
[49] T. Ali-dahmane, M. Adjdir, R. Hamacha, F. Villierasc, A. Benguedach, R.P.G. Weidler, Chimie (17) (2014) 1–6.
[50] G. Yang, Y. Deng, H. Ding, Z. Lin, Y. Shao, Y. Wang, Appl. Clay Sci. 111 (2015) 61–66.
[51] P. Fu, T. Yang, J. Feng, H. Yang, J. Ind. Eng. Chem. 29 (2015) 338–343.
[52] F. Ghorbani, V. Younesi, Z. Mehraban, M.S. Celik, A.A. Ghoreyshi, M. Anbia, J. Taiwan Inst. Chem. Eng. 44 (2013) 821–828.
[53] T. Liou, Chem. Eng. J. 171 (2011) 1458–1468.
[54] Y. Ma, H. Chen, Y. Shi, S. Yuan, Mater. Res. Bull. 77 (2016) 258–264.
[55] M. Bhagiyalakshmi, L.J. Yun, R. Anuradha, H.T. Jang, J. Hazard. Mater. 175 (2010) 928–938.
[56] D. Li, H. Min, X. Jiang, X. Ran, L. Zou, J. Fan, J. Colloid Interface Sci. 404 (2013) 42–48.
[57] B.A. Shah, A.V. Patel, M.I. Bagia, A.V. Shah, Int. J. Appl. Chem. 13 (3) (2017) 497–514.
[58] G. Lawrence, A.V. Baskar, M.H. El-Newehy, W.S. Cha, S.S. Al-Deyab, A. Vinu, Sci. Technol. Adv. Mater. (2015), http://dx.doi.org/10.1088/1468-6996/16/2/024806.
[59] Advanced Chemical Supplier, http://www.acsmaterial.com/ (Accessed June, 2017).